Fiber Optic Cables for Land Deformation Sensing

An optical fiber can be strained either mechanically or thermally, or both. As such, temperature cables are usually deployed along with strain cables so that the readings measured from strain cables can be compensated and the actual mechanical strain can be obtained. Because distributed temperature sensing using temperature cables has been well known as DTS, the authors focus on strain cables in this section.

Table 1. Three specially designed fiber optic strain cables for land deformation sensing.

Cable	NZS-DSS-C07	NZS-DSS-C02	NZS-DSS-C08
Type	Polyurethane-coated strain cable	Metal-reinforced strain cable	Point-fixed strain cable
Schematic cross-section	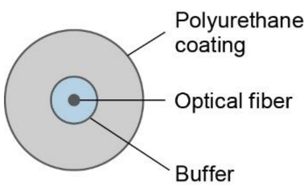	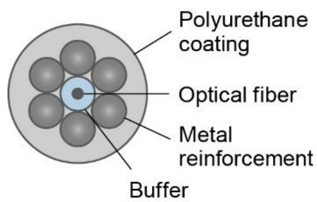	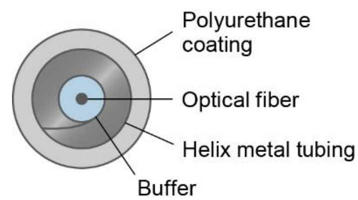
Diameter (mm)	2	5	5 (cable), 8 (fixation)
Young's modulus (GPa)	0.34	5.4	1.9
Effective stiffness (kN)[a]	1	106	37 (cable)
Features	• Can be easily prestrained and directly integrated into loose material such as soil • Can withstand moderate impacts during installation in spite of relatively low modulus	• Can survive in harsh environments due to high mechanical performance • Well suited to monitoring consolidated strata, concrete or other structures	• Measured strain is averaged between two adjacent fixations • Ideally suited for monitoring strata compaction, ground rupture (e.g., earth fissure and fault slip), or other localized large deformation (e.g., crack development)

[a]Equivalent to Young's modulus multiplied by cross-sectional area; determined under 1% tensile strain.

Strain cables for land deformation sensing should be robust enough to survive in harsh geoenvironmental and construction conditions, and ensure reliable strain transfer from the geologic material to the fiber core (Iten et al., 2008). To this aim, a couple of fiber optic strain cables have been developed (Sun et al. 2014). Table 1 lists three cables that were used in the two case studies described in this paper. The first cable is a 2 mm-diameter tight-buffed polyurethane-coated strain cable. The soft coating lowers the Young's modulus of the cable but it can still withstand moderate impacts during installation. Due to its relatively low modulus, it can be easily prestrained and directly integrated into loose material such as soil. The second cable is a 5 mm-diameter metal-reinforced strain cable. The metal reinforcements greatly increase the mechanical performance of the cable, allowing it to survive in harsh environments. This cable is well suited to monitoring consolidated strata, concrete, and other structures. The last cable is a special point-fixed strain cable. It is such a cable that the measured strain is solely dependent on the relative displacement between two adjacent fixation points; hence, the measured strain is averaged over the length between the fixation points. In the following case study, the outer diameters of the bare cable and fixation were set to 5 mm and 8 mm, respectively, and the distance between any two fixation points was 10 m. This cable is ideally suited for monitoring strata deformation, ground rupture (e.g., earth fissure and fault slip), or other localized deformation (e.g., crack development). Note that the distance between fixation points can be adjusted according to different monitoring demands.

CASE STUDY 1: LAND SUBSIDENCE IN SHENGZE

The first case study focused on the monitoring of aquifer-system compaction and associated land subsidence in Shengze, Suzhou (southern Yangtze Delta, China) (Figure 2(a)), which is one of the most developed areas in China and has been directly affected by land subsidence primarily due to groundwater extraction. According to the local land and resources department, the average subsidence of Shengze reached ~54 mm in 2007. Consequently, a borehole was drilled within the campus of Shengze Middle School to perform distributed sensing of strata compaction. The drilled borehole is 200 m deep with a 129-mm diameter. The local lithology consists almost entirely of Quaternary deposits alternating sandy, silty and clayey soils, which can be simplified as three aquifers and four aquitards (Figure 2(b)).

The three strain cables mentioned above were used in this case study. As illustrated in Figure 2(b), the cables were first attached to a cone guide. Once the borehole was drilled, the cone guide was lowered into the borehole by controlling two wire ropes. In doing this, the cables were run along the entire depth of the borehole. Afterward, the borehole was backfilled with a sand–gravel–clay mixture. Note that the cables were kept tensioned throughout the whole process. A fiber Bragg grating osmometer was deployed at 87.7 m depth (the bottom of Af II) to monitor the pore fluid pressure. It is also noted that as a first trial, the issue of thermal strain was not fully considered; therefore, temperature cables were not installed in this particular case. Because subsurface temperatures remain constant below a depth of ~15 m (Bense and Kooi, 2004), the influence of temperature on the measured strain is negligible below this depth. Finally, the cables ran from the top of the borehole to the fiber optic analyzer. The first measurement was performed in December 2012, one month after the borehole was constructed. Further details of site condition and field instrumentation can be found in Wu et al. (2016).

Typical monitored axial strains from the point-fixed strain cable and the calculated strata deformation by the direct integration of the axial strains are shown in Figures 3(a) and 3(b), respectively. First, undesirable large negative strains were observed from the near-surface zone (~0–10 m). This likely was due to the impact of the seasonal fluctuation of surface temperature (Bense and Kooi, 2004) and the unsatisfactory cable–soil coupling under low geostatic pressures (Zhang et al. 2014, 2016). The aquifer Af II at 74.4–87.7 m depth was the main aquifer for groundwater pumping in this area. The adjacent aquitard At II exhibited remarkable compressive strains, which peaked at a depth of approximately 61.2 m and decreased toward both sides of the boundary. Compressive strains were also recorded at 87.7–92.55 and 108.15–117.65 m depth within At III, but the magnitude was significantly smaller than in At II. The compressive strain observed in At II and At III was expected because the two aquitards were drained due to a hydraulic head difference resulted from groundwater extraction in Af II, which reduced the pore fluid pressure and led to the compaction. However, the deformation response of the aquifers was different from the aquitards (Figure 3(b)). As expected, Af II had deformation almost synchronous with pore fluid pressure variation, due to the large permeability of aquifers. Generally, the compaction of Af II was observed from March through September compared with some rebounds in other months. This likely was due to the larger water consumption during the warmer seasons of the year. In contrast, the aquitard At II had much more compaction than the pumping Af II but negligible rebound deformation. This could be due to the high compressibility and low permeability of aquitards.

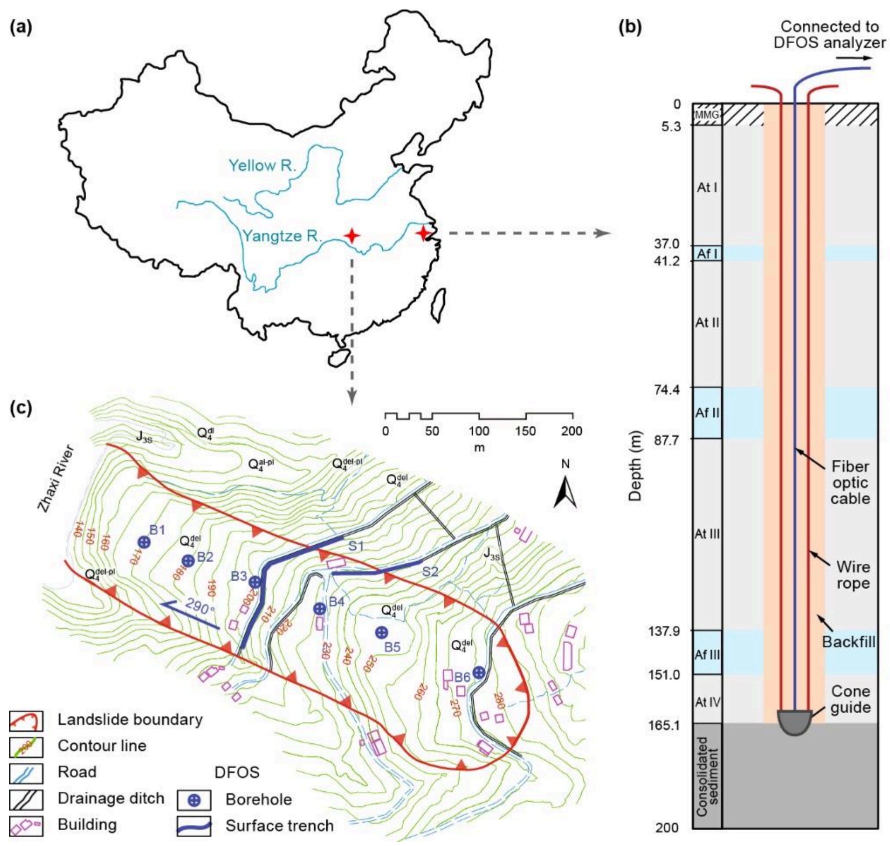

Figure 2. Description of two case studies in China: (a) locations of study areas; (b) simplified stratigraphy and schematic of fiber optic cable deployment in a borehole (Case 1—the Shengze land subsidence, southern Yangtze Delta); (c) a topographic map showing the distribution of boreholes and surface trenches where fiber optic cables were installed (Case 2—the Majiagou landslide, Three Gorges Reservoir region). MMG: man-made ground; At: aquitard; Af: aquifer.

CASE STUDY 2: THE MAJIAGOU LANDSLIDE

This particular case study focused on the monitoring of the Majiagou landside, which is situated in the Three Gorges Reservoir region, central China (Figure 2(a)). This landslide was reactivated due to the impoundment of the Three Gorges Reservoir commencing in 2003, together with abundant rainfalls in this region. It has a length of approximately 540 m, a width of

150 m, and an average slope of 15°, with its volume being ~3.1 million m^3. The lithology consists of upper Quaternary deposits with a thickness of approximately 11–16 m and the underlying thick quartz sandstones interbedded with thin silty mudstones.

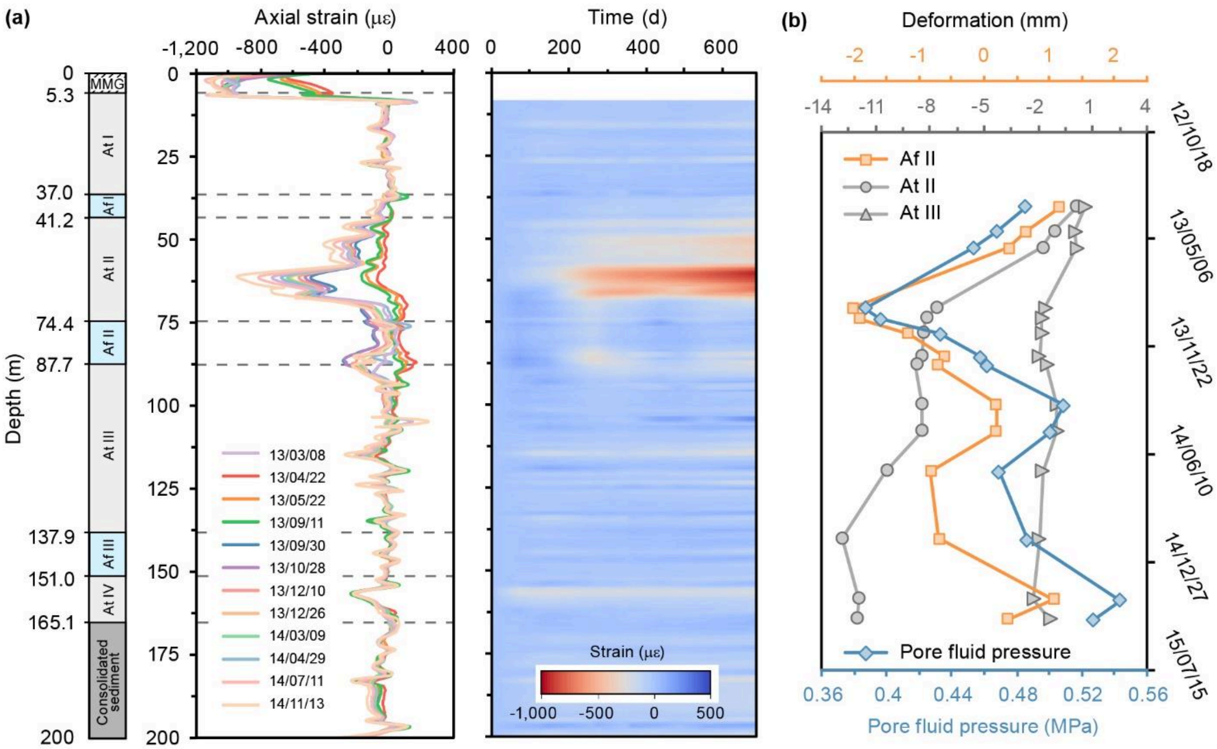

Figure 3. Results for Case 1—the Shengze land subsidence (modified from Wu et al. 2016): (a) monitored axial strain profile; (b) calculated deformation of aquifer and aquitard units.

In 2007, measures including anti-sliding piles and drainage channels were implemented to control the landslide, but the hillslope was still sliding (~15 cm/yr at middle slope during 2008–2009). Therefore, a fiber optic sensor network was established in August 2012 to obtain multi-field information of the landslide (Sun et al. 2014). Fiber optic strain and temperature cables, as well as fiber Bragg grating temperature and pore fluid pressure sensors, were installed in vertical boreholes and surface trenches, as illustrated in Figure 2(c). Note that the strain cables were polyurethane-coated strain cables, including both soil embedment and that fixed to the inclinometer casing. The analyzer used in this case and its settings were identical to Case Study 1. The first strain measurements were carried out on 9 September 2012. Further details of geologic background and sensor deployment can be found in Sun et al. (2016) and Zhang et al. (2018).

Typical monitored axial strains from a soil-embedded strain cable in borehole B4, which is 226 m in elevation and 43 m in depth, over a one-year period from September 2012 through September 2013 are presented in Figure 4(a). Two evident strain peaks were registered at depths of approximately 12.5 and 33.7 m. This indicated two sliding surfaces—the shallower one occurred at the contact between surface deposits and bedrock, while the deeper one occurred within bedrock (probably in a weak mudstone layer). Interestingly, at a depth of approximately 21.8 m, there was a minor peak which could be a third sliding surface or imply a localized shear deformation. Figure 4(b) shows the strain at 33.7 m depth and the displacement of the sliding mass along the deeper sliding surface, which was calculated using a simple kinematic method (the law of cosines). The calculated displacements from the fiber optic strains compared well with inclinometer measurements in the same borehole. The landslide movement appeared to be correlated to the reservoir water level in terms of average change. The movement was slow (~5 cm over the year) and steady, indicating that the landslide was slowly creeping.

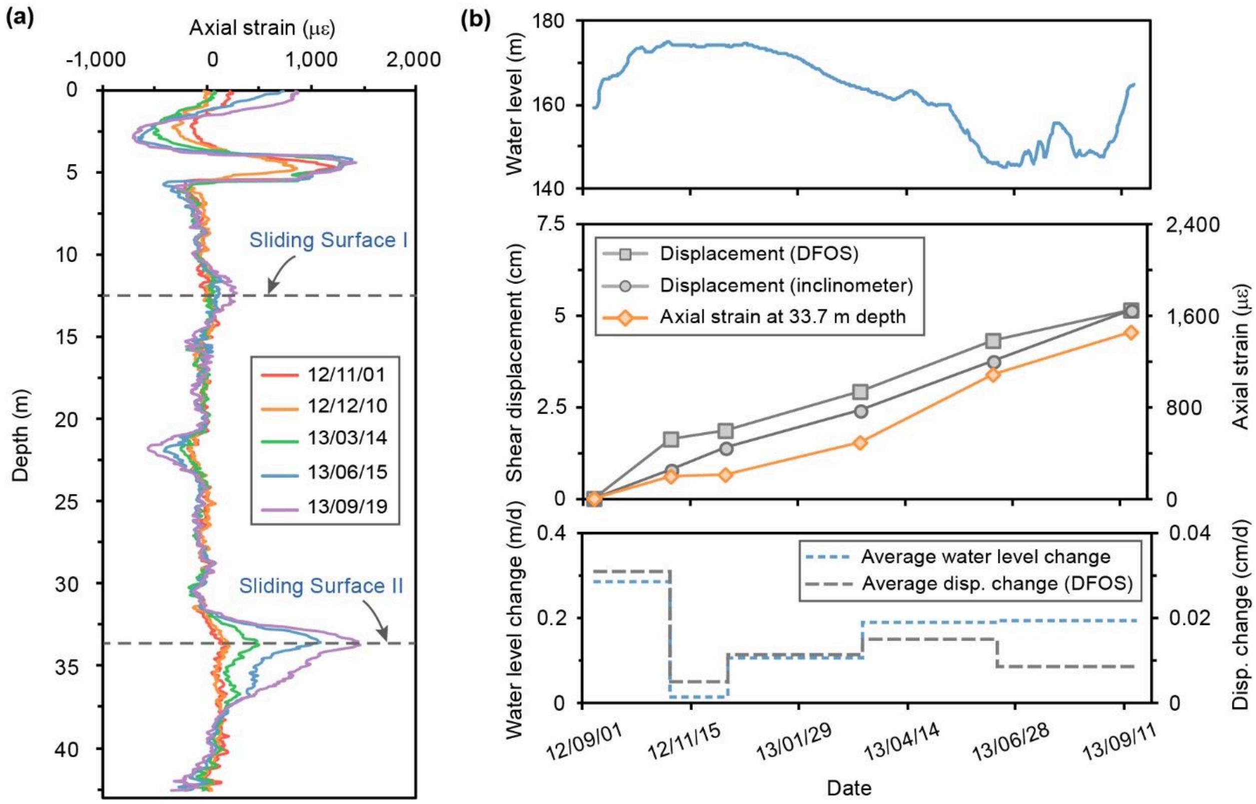

Figure 4. Results for Case 2—the Majiagou landslide (modified from Zhang et al. 2018): (a) monitored strain profile; (b) landslide deformation–time history together with the variation of reservoir water level.

CONCLUSIONS

The DFOS technology was introduced with a particular emphasis on BOTDR. The application of this technology for monitoring two typical land deformations (groundwater extraction-induced land subsidence and reservoir-induced landslide) in China was presented. The main findings of this study are the following:

- DFOS with BOTDR can complement with other conventional methods for monitoring land deformation, with the main advantage being that a complete strain profile can be obtained along a single fiber optic cable.
- Case Study 1—the Shengze land subsidence. The distributed fiber optic data showed that the main pumping aquifer Af II had deformation almost synchronous with pore fluid pressure variation, whereas the adjacent aquitard At II had delayed compaction and contributed primarily to the land subsidence.
- Case Study 2—the Majiagou landslide. The axial strain profile identified two sliding surfaces: the shallower one occurred at the contact between surface deposits and bedrock, while the deeper one occurred within bedrock. The calculated displacement along the deeper sliding surface compared well with inclinometer measurements, both indicating

that the landslide was slowly creeping.

Suggested directions for future research include the need for: a high-performance yet affordable fiber optic analyzer; standards and guidelines for the deployment of DFOS systems in the field (in particular a standardized procedure for cable installation); an effective approach for analyzing huge data sets; and the evaluation of the cable–soil interaction for a better interpretation of monitored data (Zhang et al. 2016).

ACKNOWLEDGMENTS

We thank all the fellows from Nanjing University and Nanzee Sensing, who have been actively involved in the Shengze land subsidence and Majiagou landslide monitoring projects. This work was supported by the National Natural Science Foundation of China (NSFC) grants 41427801 and 41230636 to B.S., and the Nanjing University Innovation and Creative Program for PhD Candidate grant CXCY17-24 to C.-C.Z., along with a scholarship from the China Scholarship Council through agreement 201706190165.

REFERENCES

Angeli, M.-G., Pasuto, A., and Silvano, S. (2000). “A critical review of landslide monitoring experiences.” *Engineering Geology*, 55(3), 133-147.

Bao, X., and Chen, L. (2012). “Recent progress in distributed fiber optic sensors.” *Sensors*, 12(7), 8601-8639.

Bense, V. F., and Kooi, H. (2004). “Temporal and spatial variations of shallow subsurface temperature as a record of lateral variations in groundwater flow.” *Journal of Geophysical Research: Solid Earth*, 109(B4), B04103.

Crosetto, M., Crippa, B., Biescas, E., Monserrat, O., Agudo, M., and Fernández, P. (2005). “Land deformation measurement using SAR interferometry: state-of-the-art.” *Photogrammetrie Fernerkundung Geoinformation*, 2005(6), 497-510.

Galloway, D. L., and Burbey, T. J. (2011). “Review: Regional land subsidence accompanying groundwater extraction.” *Hydrogeology Journal*, 19(8), 1459-1486.

Huntley, D., Bobrowsky, P., Zhang, Q., Sladen, W., Bunce, C., Edwards, T., Hendry, M., Martin, D., and Choi, E. (2014). “Fiber optic strain monitoring and evaluation of a slow-moving landslide near Ashcroft, British Columbia, Canada.” *Landslide Science for a Safer Geoenvironment*, K. Sassa, P. Canuti, and Y. Yin, eds., Springer, Cham, 415-421.

Iten, M., Puzrin, A. M., and Schmid, A. (2008). “Landslide monitoring using a road-embedded optical fiber sensor.” *Proc. SPIE 6933, Smart Sensor Phenomena, Technology, Networks, and Systems*, W. Ecke, K. J. Peters, and N. G. Meyendorf, eds., SPIE, San Diego, California, USA, 693315-693319.

Jousset, P., Reinsch, T., Ryberg, T., Blanck, H., Clarke, A., Aghayev, R., Hersir, G. P., Henninges, J., Weber, M., and Krawczyk, C. M. (2018). “Dynamic strain determination using fibre-optic cables allows imaging of seismological and structural features.” *Nature Communications*, 9(1), 2509.

Lienhart, W. (2015). “Case studies of high-sensitivity monitoring of natural and engineered slopes.” *Journal of Rock Mechanics and Geotechnical Engineering*, 7(4), 379-384.

Lindsey, N. J., Martin, E. R., Dreger, D. S., Freifeld, B., Cole, S., James, S. R., Biondi, B. L., and Ajo-Franklin, J. B. (2017). “Fiber-optic network observations of earthquake wavefields.” *Geophysical Research Letters*, 44(23), 11,792-11,799.

Michlmayr, G., Chalari, A., Clarke, A., and Or, D. (2017). “Fiber-optic high-resolution acoustic

emission (AE) monitoring of slope failure." *Landslides*, 14(3), 1139-1146.
Moore, J. R., Gischig, V., Button, E., and Loew, S. (2010). "Rockslide deformation monitoring with fiber optic strain sensors." *Natural Hazards and Earth System Science*, 10(2), 191-201.
Murai, D., Kunisue, S., Higuchi, T., and Kokubo, T. (2013). "In-situ formation compaction monitoring in deep reservoirs by use of fiber optics." *EGU General Assembly 2013*, Vienna, Austria, EGU2013-3860.
Picarelli, L., Damiano, E., Greco, R., Minardo, A., Olivares, L., and Zeni, L. (2015). "Performance of slope behavior indicators in unsaturated pyroclastic soils." *Journal of Mountain Science*, 12(6), 1434-1447.
Schenato, L., Palmieri, L., Camporese, M., Bersan, S., Cola, S., Pasuto, A., Galtarossa, A., Salandin, P., and Simonini, P. (2017). "Distributed optical fibre sensing for early detection of shallow landslides triggering." *Scientific Reports*, 7(1), 14686.
Shi, B., Sui, H., Liu, J., and Zhang, D. (2006). "The BOTDR-based distributed monitoring system for slope engineering." *Proceedings of 10th IAEG International Congress*, Geological Society of London, Nottingham, UK, 683.
Soga, K., and Schooling, J. (2016). "Infrastructure sensing." *Interface Focus*, 6(4), 20160023.
Sun, Y., Zhang, D., Shi, B., Tong, H., Wei, G., and Wang, X. (2014). "Distributed acquisition, characterization and process analysis of multi-field information in slopes." *Engineering Geology*, 182, 49-62.
Wang, B., Li, K., Shi, B., and Wei, G. (2009). "Test on application of distributed fiber optic sensing technique into soil slope monitoring." *Landslides*, 6(1), 61-68.
Wu, J., Jiang, H., Su, J., and Shi, B. (2016). "DFOS-based monitoring on Quaternary sediments deformation and land subsidence in Suzhou, China." *Journal of Engineering Geology*, 24(1), 56-63. (in Chinese)
Zhang, C.-C., Zhu, H.-H., Liu, S.-P., Shi, B., and Zhang, D. (2018). "A kinematic method for calculating shear displacements of landslides using distributed fiber optic strain measurements." *Engineering Geology*, 234, 83-96.
Zhang, C.-C., Zhu, H.-H., and Shi, B. (2016). "Role of the interface between distributed fibre optic strain sensor and soil in ground deformation measurement." *Scientific Reports*, 6, 36469.
Zhang, C.-C., Zhu, H.-H., Shi, B., and She, J.-K. (2014). "Interfacial characterization of soil-embedded optical fiber for ground deformation measurement." *Smart Materials and Structures*, 23(9), 095022.
Zhu, H.-H., Shi, B., Zhang, J., Yan, J.-F., and Zhang, C.-C. (2014). "Distributed fiber optic monitoring and stability analysis of a model slope under surcharge loading." *Journal of Mountain Science*, 11(4), 979-989.

Enhanced Analysis of Landslide Failure Mechanisms in the Ozark Plateau Region with Electrical Resistivity Tomography

Weston J. Koehn, S.M.ASCE[1]; Stacey E. Tucker-Kulesza, M.ASCE, P.E., Ph.D.[2]; Vanessa LeBow[3]; Salman Rahimi[4]; Michelle L. Bernhardt, Ph.D.[5]; and Clinton M. Wood, Ph.D.[6]

[1]Kansas State Univ., Dept. of Civil Engineering, 2118 Fiedler Hall, Manhattan, KS 66506. E-mail: koehnw@ksu.edu
[2]Kansas State Univ., Dept. of Civil Engineering, 2118 Fiedler Hall, Manhattan, KS 66506. E-mail: sekulesza@ksu.edu
[3]Univ. of Arkansas, Dept. of Civil Engineering, 4190 Bell Engineering Center, Fayetteville, AR 72701. E-mail: vaburges@uark.edu
[4]Univ. of Arkansas, Dept. of Civil Engineering, 4190 Bell Engineering Center, Fayetteville, AR 72701. E-mail: srahimi@uark.edu
[5]Univ. of Arkansas, Dept. of Civil Engineering, 4190 Bell Engineering Center, Fayetteville, AR 72701. E-mail: mlbernha@uark.edu
[6]Univ. of Arkansas, Dept. of Civil Engineering, 4190 Bell Engineering Center, Fayetteville, AR 72701. E-mail: cmwood@uark.edu

ABSTRACT

Landslides are a globally occurring geologic hazard that affect infrastructure such as roadways constructed in steep mountainous terrain. In the Ozark Plateau portion of Arkansas, the combination of sloping bedrock, decomposition of shale into high PI clays, and high rainfall contribute to the formation of a significant number of landslides that impact transportation infrastructure. There are currently 175 active landslides affecting roadways in Arkansas. This case history employed electrical resistivity tomography (ERT) across a recurring landslide zone within this portion of Arkansas to characterize the general stratigraphic architecture of the area. ERT surveys conducted across the slide delineated the interface between the shale bedrock and clay layer, and identified highly saturated regions above the clay/bedrock interface. Overall, the addition of ERT data to landslide investigations provides a faster and more cost effective means to develop a detailed subsurface image of the landslide compared to traditional geotechnical instrumentation alone.

INTRODUCTION

Electrical resistivity tomography (ERT) is a near surface geophysical method that measures the subsurface resistivity distribution. Hydrogeologic properties such as water content, porosity, clay content, pore fluid salinity, and pore fluid temperature control the electrical resistivity of soil and rock (Everett 2013). Numerous studies have utilized ERT to characterize the geologic framework associated with unstable slopes (Lapenna et al. 2005; Drahor et al. 2006; Gance et al. 2016; Friedel et al. 2006). ERT surveys allow for identification of lithological boundaries, providing a way to delineate potential failure zones within complex geologic environments (Perrone et al. 2014). Additionally, the extent of a failure zone can be defined as ERT surveys provide data across a wide range of spatial scales. Integration of traditional geotechnical data, such as borehole and inclinometer data, provides an enhanced characterization of the geologic framework.

The primary objectives of this study were to delineate the clay/bedrock interface and to gain insight into the main drivers behind the slope movement. Accurate slope stability analyses require a well-defined geologic framework, and the integration of geophysical data and traditional geotechnical data (borehole and inclinometer) provide the necessary information to conduct an accurate analysis of the failure.

STUDY AREA

The study area (approximately 1 km^2 in surface area) is located in the Ozark Mountain region of north-central Arkansas just south of Sand Gap, Arkansas on Arkansas Highway 7. The area sits within the Ozark National Forest, which is comprised of mountainous terrain, as a part of the Ozark Mountains, and dense hardwood and softwood vegetation (USDA 2018). The Ozark Mountains are plateaus with few folds or faults that are lifted as units and have been eroded by rising and falling rivers. The Ozarks are a part of the Boston Mountains, which are characterized by narrow V-shaped valleys and vertical bluffs of limestone and sandstone. The terrain is dominated by steep hillslopes with slope angles ranging from 10 degrees to 30 degrees. Interbedded shale and sandstone layers make up the bedrock system within the study area.

An aerial view of the study area, location of the borehole, and layout of ERT surveys are shown in Figure 1A. The study area is located adjacent to Arkansas Highway 7, which was constructed and is maintained by the Arkansas Department of Transportation (ARDOT). The site slopes from North to South and from East to West, with the lowest elevation and steepest gradient occurring near the West end of ERT line #3. The slope is moving westward, as indicated by the red and yellow arrows in Figure 1B. This has caused a caused a number of cracks to form in the pavement near the area, shown in Figure 2B, which has to be periodically repaired.

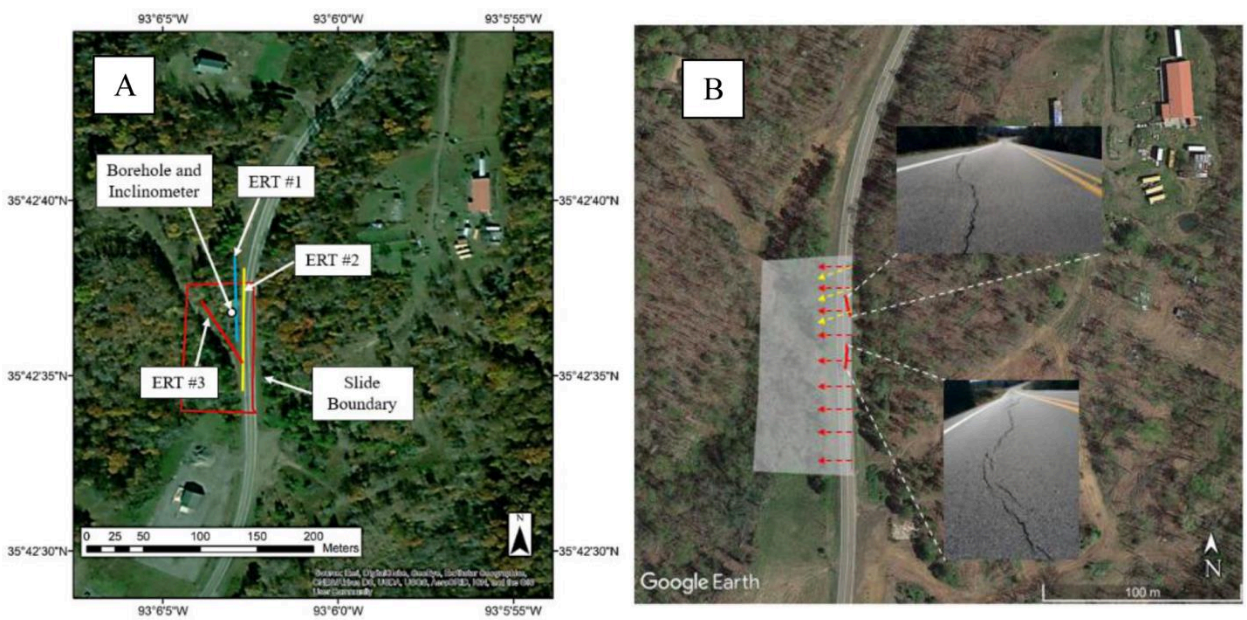

Figure 1. (A)-Overview map of study area showing the location of the ERT surveys and the borehole instrumented with an inclinometer; (B)-Location of pavement cracking within the study region and the delineated slide mass (gray polygon). The red and yellow arrows indicate the direction of the slide movement, which is predominately westward.

The boring in the area indicates that a clay/bedrock interface is present between approximately 4 m and 7 m below the ground surface. A sandstone/shale sequence make up the bedrock unit. The shale seams are highly fractured and highly weathered according to all borehole logs within the surrounding area. The top 4 m of the site is predominantly composed of a clay/gravel mixture and stiff clay. It is noted that all of the available boring logs and inclinometer data for the site are located on the West side of Highway 7 and very little information is available for the East side. Table 1 gives the layer depths and geologic description for the borehole log located on the overview map in Figure 1A.

Table 1. Borehole log giving layer depths and material description

Layer	Depth (m) Below GS	Material Description
1	0.00 - 2.90	Moist, Medium Stiff, Reddish Brown Clay with Gravel (Shale Fragments)
2	2.90 - 5.80	Moist, Stiff, Reddish Brown Clay
3	5.80 - 5.94	Sandstone with Occasional Shale Seams, Highly Weathered, Poorly Cemented, Reddish Brown and Gray
4	5.94 - 8.84	Sandstone with Frequent Shale Partings and Seams, Highly Weathered, Poorly Cemented, Frequent Fractures, Reddish Brown
5	8.84 - 11.89	Sandstone - Weathered, Cemented, Occasional Fractures, Reddish Brown
6	11.89 - 13.41	Sandstone - Weather, Cemented, Reddish Brown
	13.41	Boring Terminated

METHODOLOGY

ERT surveys are conducted by injecting electrical current into the subsurface through a pair of electrodes while simultaneously measuring the induced voltage potential across a separate pair of electrodes. Repeated sets of measurements across various electrode pairs produces an apparent resistivity pseudosection. Apparent resistivity is the resistivity of a completely homogeneous and isotropic medium, and varies based upon the type of array used to conduct the survey. All surveys must undergo inversion to produce the true resistivity distribution. The Supersting R8 from Advanced Geoscience Inc. was used to collect all datasets, and EarthImager 2D was used to invert all datasets (Advanced Geosciences Inc. 2008).

Three ERT surveys were conducted parallel and perpendicular to the slope. Figure 1A shows the location of the ERT surveys in relation to the approximate slide footprint (shown in Figure 1B). An electrode spacing of either 0.91 m or 1.52 m was used to conduct all surveys. A 56 electrode dipole-dipole/strong gradient array was used to collect all datasets within this study. A dipole-dipole/strong gradient array is an optimized array, which uses electrode configurations derived from the dipole-dipole and gradient arrays to collect data. This optimized array provides better coverage of the subsurface and a higher signal to noise ratio than the dipole-dipole array alone (Advanced Geosciences Inc. 2008). Figure 2 shows the field set up of ERT survey #1 and the location of the inclinometer at the site.

The inversion of ERT surveys is required to produce the true subsurface electrical resistivity distribution. The two statistical parameters used to quantify how well the inversion performed are the root mean square error (RMS) and the L2-norm. An estimate of the measurement noise is required prior to inversion, and is one of the stopping criteria for the inversion. A quality inversion is produced when the RMS falls below the estimated data noise, and when the L2-norm falls below 1.0 within a predefined number of iterations (8 for this study). The L2-norm should